SHAPE AND INITIAL DILUTION OF SAND ISLAND, HAWAII SEWAGE PLUME

By A. A. Petrenko,[1] B. H. Jones,[2] and T. D. Dickey[3]

ABSTRACT: The wastewater plume discharged from the Sand Island Treatment Plant, Hawaii outfall diffuser was mapped several times during September 25–October 1, 1994. The deeply submerged plume was patchy at its center, thin on its edges, and displayed vertically separated layers on three out of five days of plume mapping. Complexity of the sewage plume shape was due to a combination of factors that include temporal and spatial variations in currents, temperature stratification, and internal tides. Equilibrium depth, thickness, and initial dilution of the sewage plume were derived from in-situ measurements proximal to the sewage outfall and were compared with simulation results from the Roberts, Snyder, and Baumgartner (RSB) model. Simulated equilibrium depths were within 6 m of their measured counterparts in all but two cases, and simulated thicknesses of the plume were larger than measured thicknesses in all but two cases (out of 11 cases). Simulated dilutions were 1.9 times the dilution values derived from in-situ data. Dilution differences are explained by lack of temporal resolution in velocity measurements and differences between the engineering definition and the oceanographic characterization of initial dilutions.

INTRODUCTION

Shapes of sewage plumes are rarely observed in detail; however, the shapes are important since they are indicators of how the plume is being dispersed, which will affect its potential pollution impacts. If the plume is compact and homogeneous, its average concentration may be sufficient to estimate whether sanitary standards are achieved. But if the shape of the plume is more complex, other ways to estimate its impacts may be necessary. Sewage outfall plumes manifest a variety of shapes in the coastal environment. Off southern California, sewage plumes have often been found to be shaped as a single, though sometimes patchy, "cloud" that extends alongshore, due to forcing of the dominant alongshore currents (Jones et al. 1991; Washburn et al. 1992; Jones et al. 1993; Wu et al. 1994). In the Bosphorus Strait, the sewage plume was observed to be trapped below the interface between the denser (Mediterranean waters) and lighter (Black Sea waters) layers of the channel; sometimes it exhibited a mushroom shape close to shore where currents in the lower layer were weaker (Besiktepe et al. 1995). Several plume layers were observed at different depths around the Iona, Vancouver outfall diffuser (Faisst et al. 1990). Faisst et al. proposed two likely explanations for these observations: 1) The effluent was discharged over a depth range from 72 to 105 m leading to varying initial mixing conditions and, hence, different equilibrium depths; and 2) temporal variability in density stratification and currents led to changes in plume equilibrium depths. Multiple plume layers have also been observed with acoustic measurements (Dammann et al. 1991). Dammann et al. concluded that subsurface plumes "peeled off" from the main rising plume and remained in equilibrium on density gradients, while the main plume surfaced. Few of these studies had comprehensive data sets (including currents and density stratification) to allow full explanation of the observed plume shapes.

Dilution of sewage plumes can be estimated from in-situ measurements collected in the plume and background waters and, alternatively, can be simulated by models. In the last 10 years, only a few studies have compared measured and modeled dilution for sewage plumes (Faisst et al. 1990; Roberts and Wilson 1990; Davison et al. 1993; Roberts 1994; Wu et al. 1994). Of these studies, two included quantitative comparisons between measured and modeled dilutions. In waters off San Francisco, the Roberts, Snyder, and Baumgartner (RSB) modeled outfall dilutions were generally higher than measured dilutions by 12–20%, and modeled heights of rise were lower by 5–14% (Roberts and Wilson 1990; Roberts 1994). For the Vancouver outfall, the old version of RSB, ULINE, gave the best performance of three tested models with an average dilution of 1:471, while the field data gave an average value of 1:425 (Faisst et al. 1990). The other studies only gave qualitative results. Wu et al. (1994) found that the plume observations did not allow precise comparisons of dilutions. The conclusion of an Australian study was that the major features, i.e., initial dilution, rise height, thickness of the plume, were in agreement with predictions for a line source of buoyancy flux discharge (Davison et al. 1993; Roberts 1994).

The present study focuses on the shape and dilution of the Sand Island Treatment Plant (SITP) sewage plume. SITP is a primary treatment plant discharging an average of 284×10^6 L of treated wastewater per day in the eastern part of Mamala Bay, Honolulu, Hawaii. The sewage diffuser is located at a depth of 69–71 m, about 4 km offshore. With this location, initial dilutions of approximately 1:100 are expected during summer periods with strong stratification, and between 1:300 and 1:1000 during winter periods with weak stratification (Fischer 1979). Because bacterial contamination was regularly occurring along the eastern beaches of Mamala Bay, a general study of all potential point and nonpoint sources of pollution was organized (Colwell et al. 1995). Our component was responsible for mapping the SITP sewage plume and comparing its in-situ characteristics with modeled results. It is crucial that modeled dilution be checked against in-situ observations because risk assessment decisions are frequently based on modeled dilutions. Detailed field studies, dilution calculations, and comparisons with model results, such as those presented in this paper, are essential for testing of models used for water-quality assessment.

METHODS

In-Situ Measurements

In-situ measurements were obtained between September 25 and October 1, 1994 using an instrumented towyo platform

[1]Consultant, Dept. of Marine Sci., Univ. of Connecticut, Groton, CT 06340-6097.

[2]Res. Assoc. Prof., Dept of Biol. Sci., Allan Hancock Found., Univ. of Southern California, Los Angeles, CA 90089-0371.

[3]Prof., Oc. Phys. Lab., ICESS, UCSB, Santa Barbara, CA 93106-3060.

Note. Discussion open until November 1, 1998. To extend the closing date one month, a written request must be filed with the ASCE Manager of Journals. The manuscript for this paper was submitted for review and possible publication on November 26, 1996. This paper is part of the ***Journal of Hydraulic Engineering***, Vol. 124, No. 6, June, 1998. ©ASCE, ISSN 0733-9429/98/0006-0565–0571/$8.00 + $.50 per page. Paper No. 14743.

that carried conductivity, temperature, and depth sensors (CTD, Sea-Bird Electronics model SBE 9/11+), a beam transmissometer at 660 nm with a 0.25 m pathlength (Sea Tech, Inc.) (Bartz et al. 1978), and a chlorophyll-sensitive fluorometer (Bartz et al. 1988). Other instruments included a nine wavelength absorption-attenuation meter (WETLabs AC-9), a spectral fluorometer (WETLabs SAFire) and a particle size analyzer (CILAS). These latter instruments provided additional characterization of effluent and naturally occurring particles, as described elsewhere (Petrenko et al., to be published, 1997).

Two primary modes of sampling were used during the cruise. On the map of the eastern part of Mamala Bay, A is the location of casts 2–11 and B the location of cast 1 (Fig. 1). C is the location of mooring D2, detailed later in this paper. Isobaths correspond to depths of 15, 25, 50, 100, 200, 300, 400, and 500 m. Vertical profile data were collected while the research vessel R/V Kila (University of Hawaii) maintained station position at location A. Towyo transects were obtained by winching the platform between the surface and the bottom as R/V Kila moved forward at a speed of 1–1.5 m/s^{-1}, resulting in a depth-varying sawtooth pattern with a horizontal resolution of approximately 250 m at middepth and a vertical resolution of at least 0.5 m. The sewage plume, indicated by the stippled areas, was characterized by low salinity and high beam attenuation coefficient at 660 nm ($c660$) compared to background waters (Fig. 2). Casts 3 and 4 originate from the same profile (Fig. 2), as indicated in Table 1. Signatures in salinity and $c660$ allowed mapping of the sewage plume in 2 and 3 dimensions, using extrapolated data between towyo casts. Detailed information on the towyos and stations can be found elsewhere (Jones et al. 1995). The analysis of dilution was made using casts, either the up or down portion of towyo

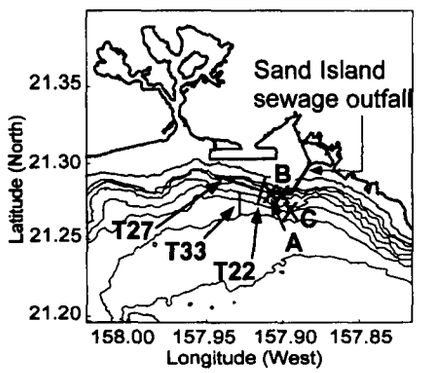

FIG. 1. Map of Eastern Part of Mamala Bay

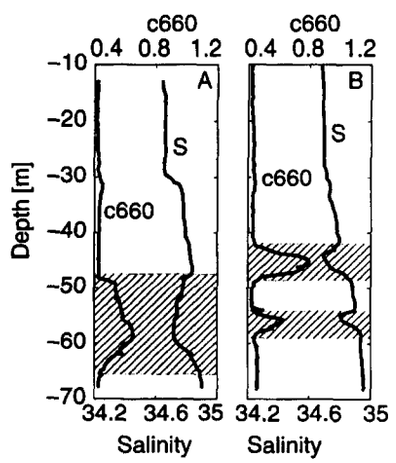

FIG. 2. Vertical Profiles of Salinity (S) and $c660$ versus Depth A, for Cast 11; B, for Casts 3 and 4

TABLE 1. Subset of Data Selected for Dilution Study

Casts (1)	Log number (2)	Profiles (3)	Date (4)	Time (5)
1	Towyo 4	Upcast 8	9/25	17:30
2	Towyo 16	Upcast 5	9/27	14:00
3	Towyo 27	Upcast 16	9/28	17:30
4	Towyo 27	Upcast 16	9/28	17:30
5	Station 9	Downcast	9/29	17:00
6	Station 9	Upcast	9/29	17:00
7	Station 11	Upcast	9/29	18:00
8	Station 13	Upcast	9/30	9:30
9	Towyo 31	Downcast 2	10/01	11:00
10	Station 17	Downcast	10/01	13:00
11	Station 19	Downcast	10/01	13:00

transects or vertical profiles. These casts were collected at the center (cast 1) or over the western end of the diffuser (casts 2–11), where the highest effluent concentrations were found (Table 1; Fig. 1).

Mooring D2, deployed by Science Applications International Corporation (SAIC) just south of the sewage outfall diffuser on the 75 m isobath (Fig. 1; location C), included a taut-wire-moored Aanderaa thermistor string and a bottom-mounted 300-kHz uplooking acoustic Doppler current profiler (Hamilton et al. 1995). Thermistors were spaced at 5-m depth intervals between 13 and 63 m, and horizontal current measurements were binned at 2 m intervals from 7 to 65 m. Temperature and currents were sampled at 30-min intervals. Froude number was calculated with the following relationship:

$$F = u^3/b$$

where u = D2 current speed at 65 m (5 m above diffuser depth) and b = specific buoyancy flux per unit length of diffuser; $b = gq\Delta\rho/\rho$, where g = standard acceleration of gravity, q = effluent volume flux per unit length of diffuser, and $\Delta\rho/\rho$ = fractional density difference, with ρ ambient density and $\Delta\rho/\rho$ the difference in density between the ambient water and the wastewater (Roberts 1977).

Modeling

Characteristics of the plume close to the diffuser were modeled with the RSB model (Roberts 1995). The RSB model uses time series of current direction and speed at 65 m, density stratification based on mooring temperature measurements (i.e., with simulated salinity), and discharge flow rates to predict the initial mixing length (IML, in meters) (Baumgartner et al. 1994). IML is the distance from the diffuser at which the wastewater plume is referred to as "established" and at which mixing starts to be dominated by the ambient turbulence; IML corresponds to the downstream end of the "near-field" or "initial mixing region." At this location, the model also provides (1) the height of rise of the plume, from which the plume equilibrium depth, Zmo_1, can be calculated by subtracting the height of rise to the total depth; (2) the thickness of the plume, Hmo_1; and (3) the plume minimum dilution, Dmo_1.

The model was also used similarly as before but based on density calculated with in-situ temperature and salinity. This was done at discrete intervals for the casts indicated in Table 1. The discrete model results, Zmo_2, Hmo_2, and Dmo_2, were compared with the in-situ plume characteristics and dilution calculated as described next.

Dilution Calculation Method

Natural tracers associated with a sewage plume can in principle be used to estimate plume dilution. The present dilution method utilizes the natural tracers, temperature (T) and salinity

(*S*), and their graphical representation, on a *T-S* diagram, with initial mixing lines between wastewater and ambient waters (Washburn et al. 1992). Once wastewater (with characteristics *Te* and *Se*) is discharged from the outfall diffuser, it first mixes with the ambient waters (with characteristics *Ta* and *Sa*) present at the depth of the diffuser. When two water masses mix, the characteristics of the resulting mixed water mass, *Tm* and *Sm*, correspond to an intermediate point on the initial mixing line joining the two end members. *Sm* and *Tm* vary depending on the dilution factor between the effluent and the ocean end member. For a given dilution *D*, between (*D*-1) unit volumes of ambient waters and 1 unit volume of wastewater, *Sm* and *Tm* of the mixed water mass are given by (Fischer 1979)

$$Sm = Sa\frac{(D-1)}{D} + \frac{Se}{D} \quad (1)$$

$$Tm = Ta\frac{(D-1)}{D} + \frac{Te}{D} \quad (2)$$

Wastewater, because of its low density relative to seawater at diffuser depth, rises in the water column until it surfaces or achieves equilibrium density beneath the surface. In the present study, the wastewater endpoint is defined as *Se* = 5.1 practical salinity scale (pss; a salinity of 35.00 g/kg, formerly written as 35.00‰, corresponds to 35.00 pss; "Tenth" 1981) and *Te* = 26.2°C. *Se* and *Te* are the averaged wastewater salinity and temperature for four quarterly samplings (October 1993, and February, June, and November 1994) (Fujioka and Loh 1995). At high-dilution values, variations in the values of the effluent endpoint, *Te* and *Se*, are negligible compared to variations in the values of *Sa* and *Ta* [see (1) and (2)]. Most of the mixing is considered to take place during the plume rise over the outfall diffuser and is referred to as initial mixing. The data show that some of this initial mixing occurs with ambient waters originating within a 10-m depth range (65–75 m) centered at the outfall diffuser depth (70 m) (Fig. 3). The two pairs of ambient end members, *Ta* and *Sa*, are from depths of 65 and 75 m and are unaffected by wastewater. The range of *Ta* and *Sa* within these pairs accounts for natural variability in ambient conditions.

Initial mixing lines are drawn between the wastewater endpoint (*Te* and *Se*, off scale in Fig. 3) and the two points (*Ta* and *Sa*) that define the range of ambient water types near the diffuser (Fig. 3). The closer the point *Tm* and *Sm* is to the endpoints *Ta* and *Sa*, the higher the dilution of the effluent with ambient waters. Effluent dilutions were at least 1:90 in this study; hence *Tm* and *Sm* were much closer to ambient water values than to effluent values. Points of equal dilutions (e.g., *D* = 80, 100, 120, 140, 160, 180, and 200) on these two mixing lines bracket zones of initial dilutions (Fig. 3). Lines of constant density anomaly (in kg/m^{-3}) are labeled 22, 22.5, 23, and 23.5. For each cast, the dilution method consists of plotting the measured *T-S* data on the *T-S* diagram with the initial mixing lines and the dilution zones. The *T-S* data exhibit an approximately linear relation from surface waters (high *T* and low *S*) to deep waters (lower *T* and higher *S*), apart from the salinity minimum due to the plume (Fig. 3). Empirical estimation of dilution comes from the observational evidence that *T-S* points in the plume are formed by simple end-member mixing between *Te*, *Se* and *Ta*, *Sa*. When the plume *T-S* data fall into an initial dilution zone, the lowest dilution reached by these *T-S* data corresponds to the minimum initial dilution of the plume (as in Fig. 3A). If they are located off the initial mixing lines (as in Fig. 3B), it indicates that the plume has already started to mix with waters shallower than the 65–75 m ambient waters. In both cases, depths corresponding to the lowest salinities of the plume are taken as the in-situ equilibrium depth of the sewage plume (*Zme*).

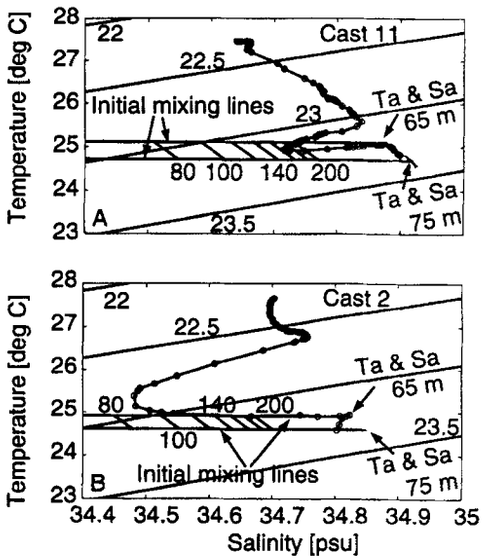

FIG. 3. Temperature-Salinity (*T-S*) Diagrams A, for Cast 11; B, for Cast 2.

RESULTS

The plume was found mostly west of the diffuser and always trapped below 40 m (e.g., Fig. 4). Three-dimensional quasisynoptic mapping of the plume was obtained by interpolating data between towyo down- and up-casts to generate sections of, for example, *c*660 during cross-shelf towyo 22 [obtained between 1:25 p.m. (A) and 1:50 p.m. (B) on September 28, 1994] and alongshore towyo 27 [obtained on the same day between 4:45 p.m. (C) and 5:30 p.m. (D)] (Fig. 4). The *x*-axis parallels the direction of the 70-m isobath alongshore (positive eastward), and the *y*-axis the cross-shelf direction (positive toward shore). Location (0,0) corresponds to the western end of the Sand Island sewage diffuser. The high spatial resolution of the measurements provided a clear view of the plume position and concentration. Variations in currents and temperature stratification during the 4-h interval separating the beginning of towyo 22 (A) and the end of towyo 27 (D) resulted in the difference in plume depths observed close to the diffuser (Fig. 4). Semidiurnal internal tides were found to be a dominant forcing in these variations of plume depths (Petrenko et al., to be published, 1997). The plume was observed to be patchy, even at its center close to the diffuser (Fig. 4). Its thickness ranged from about 20 m down to 1 m at its edge during towyo 33 (Fig. 5). Longitude is approximately constant, so *c*660 is plotted versus depth and mean latitudinal distance for each down- and up-cast. Upcasts are indicated in bold

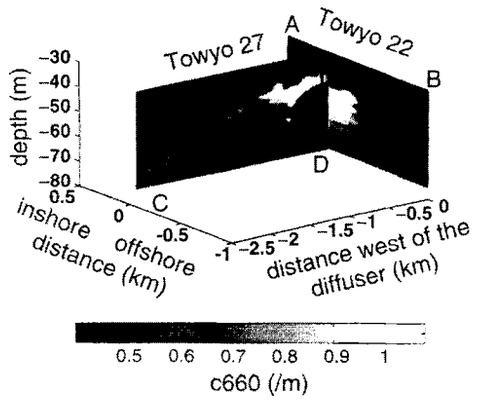

FIG. 4. Sections of *c*660 during Cross-Shelf Towyo 22 and Alongshore Towyo 27

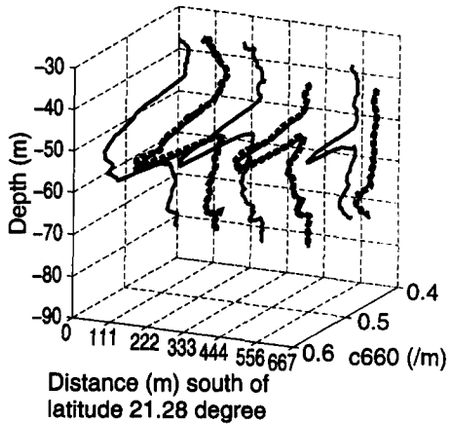

FIG. 5. Profiles of *c*660 during Cross-Shelf Towyo 33

squares to contrast with the adjacent downcasts. At distance 0 (latitude 21.28°), fresh plume is located between 45 and 65 m (Fig. 5). The plume narrows down to a few meters 250 m further south and is not detectable 650 m south of the first downcast. Below the fresh plume, a lower *c*660 signal indicates an older plume. In general, the plume was detectable at least 2–3 km west of the diffuser (Fig. 4). The plume was also found as far as 2 km south of the diffuser on September 25, and detected 500 m south of the diffuser (during alongshore towyos) on September 26 and 27 (data not shown). On these latter two days, no attempt was made to follow the plume further south so the offshore extent of the plume remained unknown. The plume was not found inshore of the 40-m isobath, probably because it was deeply submerged and the currents tended to flow parallel to isobaths rather than across topography. Multiple plumes were observed on three of the five days of plume mapping (e.g., Fig. 2B).

Time series of temperature and currents at D2 exhibited strong variability during the cruise (Hamilton et al. 1995; Jones et al. 1995; Petrenko et al., to be published, 1997). The cruise period coincided with the longest period of stratification found between June and October 1994 (Jones et al. 1995). Currents were generally westward at depths below 35 m and eastward in the upper layer until September 29, 1994 when they too became westward (Fig. 6). The starting point of the progressive vectors is the mooring D2 (x-axis 0, y-axis 0), where the current data were measured (Fig. 6). The circles correspond to the current vectors at 15 m depth, and the stars to the current vectors at 65 m depth (i.e., 5 m above the diffuser). Spacing between stars (dots) is 1 h. It should be noted that the progressive vector plots are based on currents at D2 and must not be interpreted as water-parcel trajectories in the Lagrangian sense.

Some inputs and outputs of the RSB model are shown in Fig. 7 for the period of the cruise. The measured inputs include (A) treatment plant wastewater flow in m^3/s^{-1}, (B) temperatures at 13 m (top line) and 63 m (bottom line), partial representation of the stratification input of the model; and (C) Froude number. The modeled outputs include (D) dilution, Dmo_1; (E) equilibrium depth, Zmo_1 in m; and (F) thickness of the plume, Hmo_1 in m. The corresponding measured values for (D) *Dme*; (E) *Zme*; and (F) *Hme* are represented by dots at the time of the cast measurements, indicated by the vertical dashed lines and their respective cast number(s). The Froude number reflected the current variability (Fig. 7C), and averaged 4.7 during the period from September 24 to October 1. Rapid variations of temperature stratification and velocity above the sewage diffusers (Figs. 7B and 7C) resulted in variability in outputs of the RSB model (Figs. 7D–7F). Zmo_1 varied between 40 and 60 m below the surface (indicated in negative values in Fig. 7E) during the cruise. Zmo_1 rose above 50 m only during weak stratification (when temperature difference between 13 and 63 m was 1° or less) (Fig. 7B). Continuous Dmo_1 based on temperature and simulated salinity (Fig. 7D) were about 1.5 times discrete Dmo_2 based on in-situ temperature and salinity (Table 2), and about 2.6 times dilutions derived from the *T-S* technique, *Dme* (Table 2).

Analysis was focused on comparing the measured plume characteristics and the simultaneous discrete model results (Table 2). On average, Dmo_2 values were about 1.9 times *Dme* values (first quartile average: 1.1; fourth quartile average: 2.6).

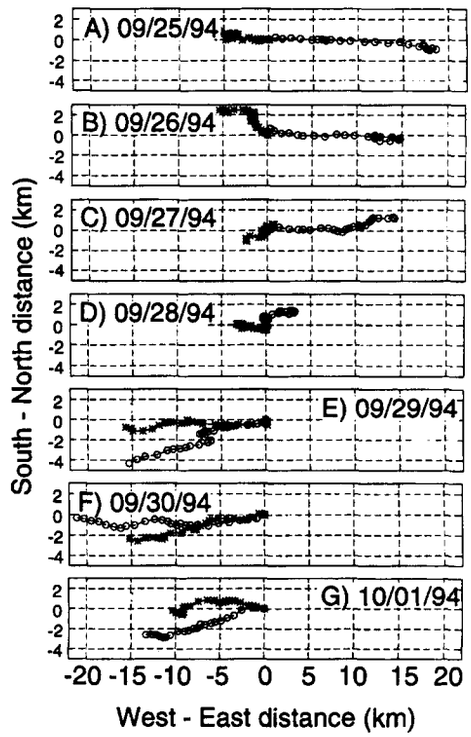

FIG. 6. Progressive Vector Diagrams for 24-h Period on Each Day of Cruise A, 09/25; B, 09/26; C, 09/27; D, 09/28; E, 09/29; F, 09/30; G, 10/01, 1994

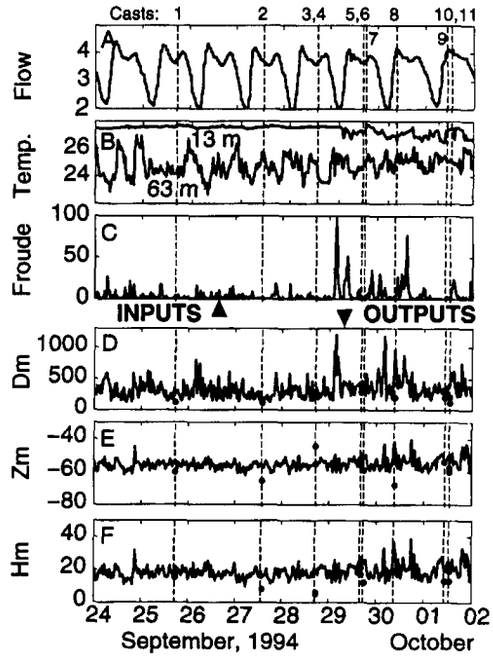

FIG. 7. Some Inputs and Outputs of RSB Model

TABLE 2.

Cast (1)	Zme (2)	Zmo_2 (3)	Hme (4)	Hmo_2 (5)	F (6)	Dme (7)	Dmo_2 (8)
1	−60	−57	15	17	0.94	90	203
2	−65	−59	8	12	0.00	—	116
3	−44	−58	6	16	1.89	—	292
4	−55	−58	5	16	1.89	—	292
5	−56	−51	21	21	0.11	200	238
6	−53	−49	17	23	0.11	185	273
7	−59	−55	12	19	1.01	250	245
8	−68	−56	19	18	6.01	180	425
9	−54	−57	13	17	2.66	140	301
10	−60	−55	13	19	3.52	120	335
11	−57	−57	19	16	3.52	165	275
All	−57	−55	13	19	1.97	—	287
−2, 3, 4	−58	−56	16	18	2.23	166	272

Note: Measured (Zme) and modeled (Zmo_2) plume equilibrium depths in meters (note that negative depths indicate distance below surface), measured (Hme) and modeled (Hmo_2) plume thickness in meters, Froude number (F), and dilution derived from temperature and salinity measurements (Dme) and modeled dilution (Dmo_2). Dme cannot be calculated in cases such as casts 2, 3, and 4 (see Fig. 3B).

The greatest difference between Dme and Dmo_2 was found for cast 8, the cast with the highest F (about 6). Here the high Dmo_2 (425) was not mirrored by a similarly large Dme (180). If the values for cast 8 were excluded, Dmo_2 would be 1.8 times Dme.

During the measurement periods, Zmo_2 were all in a 10-m depth interval (49–59 m); Zme covered a 24-m depth range (44–68 m) (Table 2). Zmo_2 and Zme were within 6 m of each other in all but two cases (casts 3 and 8). Hmo_2 were larger than the measured plume thickness, Hme, in all but two cases (casts 8 and 11).

DISCUSSION

Plume Shape

The plume structure was considerably more complex (e.g., patchiness, thin edges) than the compact shape of the classical mathematical picture of a buoyant plume. Instantaneous laboratory images of plumes (Roberts et al. 1989b) and laser-induced fluorescence images (Roberts 1994) also exhibit a complex and patchy structure. It is only when averaged over time that these measurements converge toward the compact plume (often represented by a Gaussian curve) typical of model simulations. Since the towyo measurements are instantaneous snapshots for each spatial position, the shape of the observed plume is not smooth, but rather patchy. Patches of high and low concentrations in sewage plumes have been detected in-situ by acoustic measurements and referred to as "boluses" (Dammann et al. 1991). Several processes may explain the complexity of the plume shape:

1. The plume shape is more complex when current and stratification conditions result in Froude numbers (F) smaller than 10 (Roberts et al. 1989a). A wide diversity of plume shapes dependent on the F range and current direction was observed in laboratory experiments where effluent discharged into linearly density-stratified tanks with steady current of constant speed and direction (Roberts et al. 1989b). Plumes associated with F smaller than 10 are expected to exhibit an overshooting phase followed by an equilibrium phase for currents orthogonal to the diffuser and a more complex and much less compact three-dimensional structure for currents parallel to the diffuser (the case considered here).
2. Plume shapes also vary on time scales of minutes to hours in response to temporal variations in F. Patchiness at the center of the plume could result from rapid changes in currents and stratification (e.g., internal waves, solitons, wind-driven currents), modifying the equilibrium depth of the plume and creating gaps between various plume layers. When $0 < F < 10$ and cross-diffuser currents are present, momentum-driven overshooting is more likely to occur, complicating the plume shape close to the diffuser.
3. Internal tides may also contribute to the plume's spatial complexity. The plume equilibrium depth was found to follow the vertical displacements of isopycnal surfaces, which were driven by semidiurnal internal tides (Petrenko et al., to be published, 1997). Internal tides have been shown to create patchiness in naturally occurring particles such as phytoplankton biomass and species composition (Kamykowski 1974, 1976). The semidiurnal internal tides observed in Mamala Bay are expected to have a comparable influence on the shape of the plume. Internal tides can also drive internal solitary waves (Bogucki et al., in press, 1997) and potentially affect plume patchiness.
4. Variations in current shear may also contribute to the formation of several plumes. This hypothesis cannot currently be validated in the laboratory due to the experimental difficulty of creating shear conditions. As mentioned in the Introduction, multiple plumes could also be formed simultaneously if the effluent was discharged over a wide depth range with distinct temperature, salinity, and current velocity gradients. Because the Sand Island wastewater is injected at nearly constant depth (69–71 m), depth range is an unlikely explanation for the presence of several plume layers.

The in-situ plume thickness was generally smaller than the model results would predict. On days when several plumes were observed, the discrepancy could be due to the plume splitting into several layers. For example, in the case of casts 3 and 4, the summation of the two plume thicknesses provides a result closer to the modeled result (Hme = 11 m for Hmo_2 = 16 m). Another reason for the difference between measured and modeled thicknesses could be the compactness of the simulated plume; the observed patchy plume with boluses of high concentration could result in thinner or thicker layers than a more evenly distributed plume.

Dilution

On average, the RSB model Dmo_2 exceeded Dme by 90%. Dilutions estimated with the T-S diagram method represent lower bounds of dilution since the method assumes that dilution takes place with deep waters from within ±5 m of the diffuser; hence, providing smaller dilutions than if dilution takes place with shallower and less saline waters. In reality, mixing probably continued to occur with waters in the depth range from the diffuser up to the equilibrium depth. Because dilution calculation is more sensitive to the variability of salinity than to that of temperature, upper bounds for dilution were calculated using the minimum salinity observed between the bottom and the plume depth. These upper bound dilutions exceeded Dme by 10%. The modeled dilutions were on average 1.7 times these overestimated dilutions.

During the summer of 1994, very low dilutions probably never occurred for more than a few hours at the SITP outfall because strong stratification never lasted for longer than a portion of the tidal cycle (Hamilton et al. 1995). With the unusually persistent stratification present during the study period, the effluent plume remained deep (below 40 m) and initial dilutions, both Dme and Dmo_2, were generally low during the measurement casts (Fig. 7D). Dme was in the range 1:90–1:

250, slightly higher than the dilutions estimated at the design stage of the diffuser for summer conditions (Fischer 1979).

The lowest *Dme* found during the cruise was during cast 1, which was the only cast of this study taken over the middle of the diffuser. Cast 1 contains a density inversion (data not shown), indicating that the measurements may have been obtained in a still-rising plume, in which case dilution was incomplete. Only two casts (casts 1 and 8) may have been obtained in a still-rising phase. Casts 1 and 8 correspond to Dmo_2, respectively, 2.2 and 2.4 times *Dme*. Because two other casts (9 and 10) exhibit Dmo_2, respectively, 2.1 and 2.8 times *Dme* but do not contain density inversions (data not shown), differences between measured and modeled dilution cannot entirely be explained by in-situ measurements collected in a still-rising phase.

Observations and near-field model dilutions are in best agreement for periods when the water column is stratified and currents are weak (low F). For stronger currents (e.g., cast 8) the RSB model predicts dilution 2.4 times that calculated from the *T-S* diagram. As mentioned earlier, *Dme* of cast 8 may have been underestimated due to measurements in a still-rising phase; nonetheless it is doubtful that this could account for a dilution 2.4 times smaller. Since the IML predicted by the model increases with current speed, it is possible that under strong current conditions the in-situ measurements were taken closer to the diffuser than the IML distance. Under strong current conditions, in-situ measurements taken at the IML might yield a larger *Dme*, closer to Dmo_2. Moreover, currents measured at the mooring are the average of currents over 2 min. If high-velocity currents happen to coincide with these 2 min of measurements, the velocity could be falsely higher than the velocity averaged over the 30 mn separating each measurement. Since there is no way to estimate that potential bias, RSB was run with zero velocity to obtain an underestimate of the model results. In the case of cast 8, "zero velocity" Dmo_2 was 226 instead of 425; this value was closer to *Dme* (180). Dmo_2 values calculated with zero velocities were on average only 1.3 times *Dme*.

CONCLUSIONS

In oceanic environments as variable as Mamala Bay, until synoptic three-dimensional (3D) detection of outfall plumes combined with dilution calculations are technologically feasible, engineering model dilutions and oceanographic dilutions may diverge because they are not defined for the former, and calculated for the latter, at the same location. Moreover, continuous velocity measurements should be collected for further reducing potential differences between measured and modeled dilutions.

Plume behavior is extremely complex in environments where stratification is variable and current amplitudes and directions change with depth and time. Accurate and detailed representation of the oceanographic complexity is beyond the capacity of available dilution models. In the present study, the RSB results captured the gross characteristics, equilibrium depth, and thickness of the observed wastefield. Whether the discrepancies found between *Dme* and Dmo_2 in this study resulted from limitations in the model, inaccuracies in the model inputs, or uncertainties in *Dme* cannot be concluded. Studies to investigate model sensitivity to particular inputs may yield additional insights.

Near-field models have been incorporated into 3D-coupled circulation/water-quality models, which are state-of-the-art tools used for risk-assessment analyses (e.g., Blumberg and Connolly 1995). However, the simplified near-field models do not parameterize the complexity of sewage plume shapes and patchiness. Inclusion of in-situ sewage plume measurements may be necessary for the 3D models to properly define the entire range of solutions and plume characteristics.

Differences between model dilutions based on mooring temperature and simulated salinity (Dmo_1) and model dilutions based on in-situ temperature and salinity (Dmo_2) reflect the necessity to have both temperature and conductivity probes on moorings for plume dilution studies.

At the SITP site, additional field observations should be obtained during periods when temperature stratification is weak or absent to determine, first, if the plume is detectable under well-mixed conditions or if use of an artificial/added tracer is necessary for detection, and, second, whether agreement between plume characteristics derived from in-situ data and RSB-type model outputs is maintained. Validation of the RSB model or its future versions will allow more effective diffuser design in the future, as well as the extension of predictability of plume behavior for a variety of conditions for which in-situ data are not available.

ACKNOWLEDGMENTS

Funding for this research was made possible by grants from the Mamala Bay Study Commission Fund, a component trust of Hawaii Community Foundation. Additional funding was granted by the USC Sea Grant program. Special thanks go to Philip Roberts for providing RSB data and suggestions and to SAIC, especially to Peter Hamilton, for the D2 mooring data. We thank Libe Washburn for reviewing the paper and suggesting changes in dilution calculations and David Adelson for helpful suggestions regarding the manuscript. These data were collected with the assistance of the master and crew of the R/V Kila, University of Hawaii.

APPENDIX I. REFERENCES

Bartz, R., Spinrad, R., and Kitchen, J. C. (1988). "A low power, high resolution, in situ fluorometer for profiling and moored applications in water." *Oc. Optics*, 9, 157–170.

Bartz, R., Zaneveld, J. R. V., and Pak, H. (1978). "A transmissometer for profiling and moored observations in water." *Oc. Optics*, 5, 102–108.

Baumgartner, D. J., Frick, W. E., and Roberts, P. J. W. (1994). "Dilution models for effluent discharges." *600/R-93/139*, Environmental Protection Agency, Washington, D.C.

Besiktepe, S. T., Ozsoy, E., and Latif, M. A. (1995). "Sewage outfall plume in the 2-layer channel—an example of Istanbul outfall." *Wat. Sci. and Technol.*, 32, 69–75.

Blumberg, A. F., and Connolly, J. P. (1995). "Modeling transport and fate of pathogenic organisms in Mamala Bay." *Final Rep. MB-5*, Mamala Bay Commission, Hawaii.

Colwell, R. R., Orlob, G. T., and Schubel, J. R. (1995). "Study management." *Final Rep. MB-1*, Mamala Bay Commission, Hawaii.

Dammann, W. P., Proni, J. R., Craynock, J. F., and Fergen, R. (1991). "Oceanic wastewater outfall plume characteristics measured acoustically." *Chem. and Ecology*, 5, 75–84.

Davison, A., Thornton, P., and Spelman, G. (1993). "The dispersion of sewage from the deep water outfall off Malabar using radioisotope tracer techniques." *Interim report to the EPA Interim EPA*, Australian Nuclear Sci. and Technol. Org., Menai, NSW 2234, Australia.

Faisst, W. R., McDonald, M., Noon, T., and Marsh, G. (1990). "Iona outfall, plume characterization study." *Proc., 1990 Nat. Conf. on Hydr. Engrg.*, H. Chang, ASCE, New York.

Fischer, H. B., List, E. J., Koh, R. C. Y., Imberger, J., and Brooks, N. H. (1979). "Mixing in inland and coastal waters." Academic Press, Inc., New York.

Fujioka, R. S., and Loh, P. C. (1995). "Characterization of the microbiological quality of water in Mamala Bay." *Final Rep. MB-7*, Mamala Bay Commission, Hawaii.

Hamilton, P., Singer, J., and Waddell, E. (1995). "Ocean currents measurements." *Final Rep. MB-6*, Mamala Bay Commission, Hawaii.

Jones, B. H., Dickey, T. D., and Petrenko, A. A. (1995). "Plume dynamics and dispersion in Mamala Bay, HI." *Final Rep. MB-S11*, Mamala Bay Commission, Hawaii.

Jones, B. H., Dickey, T. D., Washburn, L., and Manov, D. (1993). "Physical and biological dynamics of sewage outfall plumes in the coastal region: an integrated observational approach." *Water pollution II: modeling, measuring and prediction*, L. C. Wrobel and C. A. Brebbias, eds., Computational Mechanics Inc., Southampton, U.K., 527–534.

Jones, B. H., Washburn, L., and Wu, Y. (1991). "The dispersion of ocean

outfall plumes: physical and biological dynamics." *Coast. Zone '91, Proc., 7th Symp. on Coast. & Oc. Mgmt.*, ASCE, New York, 74–85.
Kamykowski, D. (1974). "Possible interactions between phytoplankton and semidiurnal internal tides." *J. Marine Res.*, 32, 67–89.
Kamykowski, D. (1976). "Possible interactions between plankton and semidiurnal internal tides. II. deep thermoclines and trophic effects." *J. Marine Res.*, 34, 499–509.
Roberts, P. J. W. (1977). "Dispersion of buoyant waste water discharged from outfall diffusers of finite length." PhD thesis, Calif. Inst. of Technol., Pasadena, Calif.
Roberts, P. J. W. (1994). "Jets and plumes and ocean outfall design." *Recent research advances in the fluid mechanics of turbulent jets and plumes*, P. A. Davies and M. J. V. Neves, eds., Kluwer Academic, Dordrecht, Boston, London.
Roberts, P. J. W. (1995). "Near-field modeling of the Mamala Bay Outfalls." *Wat. Sci. Tech.*, 32, 159–166.
Roberts, P. J. W., and Wilson, D. (1990). "Field and model studies of ocean outfalls." *Proc., 1990 Nat. Conf. on Hydr. Engrg.*, H. Chang, ASCE, New York.
Roberts, P. J. W., Snyder, W. H., and Baumgartner, D. J. (1989a). "Ocean outfalls I: submerged wastefield formation." *J. Hydr. Engrg.*, ASCE, 115, 1–25.
Roberts, P. J. W., Snyder, W. H., and Baumgartner, D. J. (1989b). "Ocean outfalls II: spatial evolution of submerged wastefield." *J. Hydr. Engrg.*, ASCE, 115, 26–48.
"Tenth report of the joint panel on oceanographic tables and standards." (1981). *Unesco Technical Papers in Marine Sciences*, 36, 24.
Washburn, L., Jones, B. H., Bratkovich, A., Dickey, T. D., and Chen, M. S. (1992). "Mixing, dispersion, and resuspension in vicinity of ocean waste-water plume." *J. Hydr. Engrg.*, ASCE, New York, 118, 38–58.
Wu, Y. C., Washburn, L., and Jones, B. H. (1994). "Buoyant plume dispersion in a coastal environment—evolving plume structure and dynamics." *Cont. Shelf Res.*, 14, 1001–1023.

APPENDIX II. NOTATION

The following symbols are used in this paper:

$c660$ = beam attenuation coefficient at 660 nm in m^{-1};
Dme = initial dilution derived from in-situ measurements;
Dmo_1 = modeled (simulated salinity) initial dilution;
Dmo_2 = modeled (in-situ salinity) initial dilution;
F = Froude number;
Hme = measured plume thickness in m;
Hmo_1 = modeled (simulated salinity) plume thickness in m;
Hmo_2 = modeled (in situ salinity) plume thickness in m;
S = salinity in pss;
Sa = ambient salinity;
Se = effluent salinity;
Sm = mixed (between ambient and effluent) salinity;
Sme = measured salinity;
T = temperature in °C;
Ta = ambient temperature;
Te = effluent temperature;
Tm = mixed (between ambient and effluent) temperature;
Tme = measured temperature;
Zme = measured equilibrium depth in m;
Zmo_1 = modeled (simulated salinity) equilibrium depth in m; and
Zmo_2 = modeled (in situ salinity) equilibrium depth in m.